PAPER

Experimental Evaluations on Learning-Based Inter-Radar Wideband Interference Mitigation Method

Ryoto KOIZUMI[†], ***Nonmember***, **Xiaoyan WANG**[†a)], ***Member***, **Masahiro UMEHIRA**[††], ***Fellow***, **Ran SUN**[†], ***and*** **Shigeki TAKEDA**[†], ***Members***

SUMMARY In recent years, high-resolution 77 GHz band automotive radar, which is indispensable for autonomous driving, has been extensively investigated. In the future, as vehicle-mounted CS (chirp sequence) radars become more and more popular, intensive inter-radar wideband interference will become a serious problem, which results in undesired miss detection of targets. To address this problem, learning-based wideband interference mitigation method has been proposed, and its feasibility has been validated by simulations. In this paper, firstly we evaluated the trade-off between interference mitigation performance and model training time of the learning-based interference mitigation method in a simulation environment. Secondly, we conducted extensive inter-radar interference experiments by using multiple 77 GHz MIMO (Multiple-Input and Multiple-output) CS radars and collected real-world interference data. Finally, we compared the performance of learning-based interference mitigation method with existing algorithm-based methods by real experimental data in terms of SINR (signal to interference plus noise ratio) and MAPE (mean absolute percentage error).

key words: *CS radar, inter-radar interference, wide band interference, learning-based method, experimental evaluations*

1. Introduction

At present, there is a surging interest in autonomous driving technology and Advanced Driver Assistance Systems (ADAS), driven by the goal of mitigating traffic congestion and offering exceptionally convenient modes of transportation [1], [2]. Achieving autonomous driving hinges significantly on the effectiveness of onboard sensing techniques in perceiving the surrounding environment. In contrast to camera and LiDAR (Light Detection and Ranging), radar system offers cost-effectiveness and excels in resilience against adverse weather conditions, backlighting, and various other environmental factors [3]. Chirp Sequence (CS) radar, in particular, is considered a promising mainstay in onboard radar systems due to its ability to simultaneously detect distances and relative velocities of multiple targets [4]. To accurately separate and identify pedestrians, a distance resolution of approximately 0.2 meters is necessary, which translates to a required bandwidth of around 3 GHz that inversely proportional to the distance resolution [5]. Therefore, in the future it is expected that high-resolution radars in the mmWave frequency band will become widely adopted, leading to the dense utilization of numerous radars. As a result, the interference between radars due to their proliferation will become a significant issue in the future [6].

Inter-radar interference [7] can be divided into two types: wideband interference [3], which results in an increased noise level in the frequency spectrum and causes the miss detection on targets; and narrowband interference [8], which generates fake peak in the frequency spectrum and leads to false detections of non-existent targets (i.e., ghost targets). Compared to narrowband interference, wideband interference is much easier to occur. Therefore, in this study, we focus on the mitigation of wideband interference.

Wideband interference mitigation techniques have been widely investigated in recent years. Most of them detect and suppress the interference in time domain by setting a threshold to detect the interference samples, such as the conventional zero suppression method [9]. Another approach involves the application of an inverse raised cosine window to the affected portion, aiming to mitigate interference and enhance the continuity of the resulting time-domain signal [10]. In [11], the interference is mitigated by reconstructing the disrupted samples in the time-domain baseband signal by Kalman filtering. To appropriately control the interference detection threshold from the received beat signals, an advanced wideband interference mitigation technique using envelope detection and sorting has been proposed for automotive FMCW radar [12]. In [13], the authors proposed an interference mitigation method using an adaptive canceller to minimize the correlation between the waveforms of the victim and interfering radars. Besides the methos performed in time-domain, a spatial-domain detector design for mutual interference mitigation among automotive MIMO-FMCW radars was proposed in [14], and a Least Mean Squares (LMS) algorithm-based adaptive beamformer was investigated in [15].

In recent years, deep learning based methods have also been proposed and demonstrated excellent performance based on simulation results [16]–[22]. A Convolutional Neural Network (CNN)-based approach for interference mitigation on inter-radar interference was investigated in [16]. The interference mitigation in CS automotive radars via signal reconstruction based on autoregressive (AR) models in fast- and slow-time was proposed in [17]. In [18], a Fully Convolutional Network (FCN) was proposed to mitigate the inter-

Manuscript received October 6, 2023.
Manuscript revised December 14, 2023.
Manuscript publicized January 11, 2024.

[†]Graduate School of Science and Engineering, Ibaraki University, Hitachi-shi, 316-8511 Japan.
[††]Department of Electronics and Communication Technology, Nanzan University, Nagoya-shi, 466-8637 Japan.
a) E-mail: xiaoyan.wang.shawn@vc.ibaraki.ac.jp (Corresponding author)

DOI: 10.1587/transfun.2023EAP1122

ference and noise in the time-frequency spectrum obtained by the Short-Time Fourier Transform (STFT) algorithm. Instead of coping with interference directly, deep learning was also employed for the classification and detection purpose in [19]. In [20], a two-dimensional CNN working on covariance matrices of signals extracted from the region of interest as well as the information of chirp positions was proposed. In [21], [22], RNN-based automotive radar signal interference mitigation methods were proposed. Furthermore, the authors in [23] demonstrated that the wideband interference cancellation can also be carried out in frequency domain. However, all of these methods were assessed solely through simulations, leaving their real-world effectiveness uncertain.

In this paper, we evaluate the performance of the learning-based inter-radar interference mitigation method through both simulations and experiments. Specifically, we firstly assess the interference mitigation performance in terms of SINR (Signal to Interference plus Noise Ratio) and model training time through simulations in an extremely challenging environments with up to 7 interfering radars. Then, we conduct extensive experiments using multiple 77GHz MIMO (Multiple-Input and Multiple-Output) CS radars to collect real-world data from various inter-radar interference scenarios. Finally, we use this real data to validate the performance of the learning-based method and compare its performance with existing algorithm-based methods.

2. Principle of Wideband Interference in CS Radar

2.1 Principle of CS Radar

The block diagram of the CS radar and the waveform of the chirp-modulated CS radar are shown in Figs. 1 and 2, respectively. The Voltage-Controlled Oscillator (VCO) emits a sequence of chirp signals modulated by a sawtooth waveform and captures the returning signals from the target. The transmitted signal and the reflected signal are multiplied by a mixer, and then passed through a Low Pass Filter (LPF) to obtain the beat signal. The frequency of this signal, which is also called beat frequency, consists of the absolute frequency difference between the transmitted and received signal. This signal undergoes conversion through an Analog-Digital Converter (ADC), and by applying Fast Fourier Transform (FFT), we can acquire the frequency spectrum. Finally, target detection is conducted in the frequency domain by using peak detection algorithm.

The frequency of the beat signal, f_B, can be given by the following equation.

$$f_B = \frac{2R\Delta f}{c\Delta T} + \frac{2v f_0}{c} \tag{1}$$

where R represents the target's distance, v represents the target's relative velocity, c is the speed of light, Δf denotes the radar's sweep frequency, and f_0 represents the carrier frequency. The first term of Eq. (1) corresponds to the beat frequency proportional to the distance R, while the second term represents the Doppler frequency proportional to the velocity v. In CS radar, the sweep period ΔT is set to be extremely short so that the Doppler frequency becomes extremely small. Therefore, by neglecting the second term in Eq. (1), the target's distance R can be calculated by using the beat frequency f_B. Furthermore, by performing a Doppler FFT spanning multiple chirps within a frame, the phase difference between consecutive chirps can be detected, and the relative velocity v can be derived.

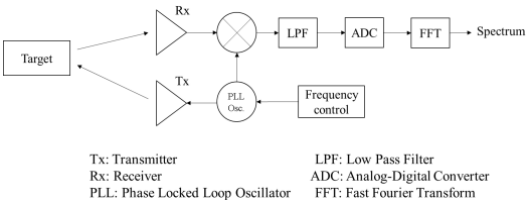

Fig. 1 Block diagram of CS radar.

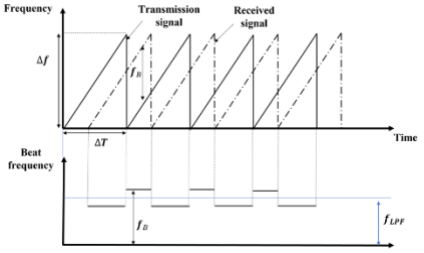

Fig. 2 Waveform of CS radar.

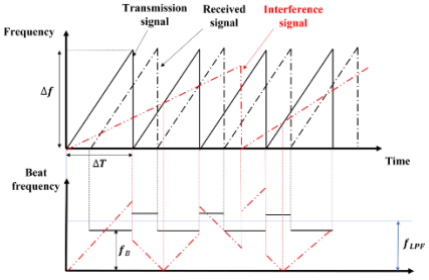

Fig. 3 Inter-radar wideband interference.

2.2 Principle of Wideband Interference

Figure 3 illustrates the principle of wideband interference for CS radars. Wideband interference is a type of inter-radar interference that arises when the chirp rate of the transmitted signal differs from that of the interfering signal. As shown in Fig. 3, besides the beat frequency of the reflected signal from the target, an additional beat frequency from the interfering radar appears, which is the absolute frequency difference between transmitted and interfering signal. Generally, the received power of the interfering signal is much greater than that of the reflected signal from the target. Therefore, when the beat frequency of the interfering radar becomes smaller than the passband of the LPF, an impulse-like interfering signal in the time domain can be observed. In the frequency spectrum of this signal, the noise level rises across the en-

tire frequency range, leading to an increase in the target's undetection rate.

3. Inter-Radar Interference Mitigation Methods

3.1 Conventional Zero Suppression Method

Zero suppression method is one of the simple yet popular approaches for mitigating inter-radar interference. Zero suppression method uses a threshold to detect the interference samples. Specifically, the threshold R_{th} is set using the average of the absolute values of the beat signal samples $r(i)$ by the following equation.

$$R_{th} = k\frac{1}{N}\sum_{i=1}^{N}|r(i)| \tag{2}$$

where N is the number of samples of the beat signal, k is a parameter to adjust the threshold. In the original beat signal, samples satisfying $R_{th} < |r(i)|$ are considered as interference, and their values will be set to 0 [12]. However, this method has a problem that it becomes difficult to detect the interference when the level of the interference signal is small.

3.2 Envelope Detection and Sorting Based Interference Mitigation Method

In order to solve the problem in the conventional zero suppression method, interference mitigation method based on envelope detection and sorting [12] has been proposed. We briefly explain the process of this method as follows. First, among the absolute values of a beat signal having N time samples, the envelope data $E(i)$ are obtained. Specifically, envelope detection uses a sliding window with window width $2W + 1$ for the absolute value $|r(i)|$ $(i = 1, 2, \ldots, N)$ of the beat signal, and calculates the maximum value from consecutive $2W + 1$ points. In the case of $i < W$ or $i > N - W - 1$, the maximum value is found from the ranges of 1 to $i + W$ and $i - W$ to N, respectively. Next, envelope $E(i)$ is sorted in ascending order, and effective range parameters a and b $(0 < a < b < 1)$ are set for calculating the average value of the desired signal. Thereafter, k times the average value of the envelope is set as the threshold R_{th}. Finally, samples satisfying $R_{th} < |r(i)|$ are regarded as interference and are set to zero. Furthermore, by using an interference mitigation sliding window, residual interference noise after zero suppression is removed.

3.3 RNN Based Interference Mitigation Method

However, the existing threshold-based methods perform poorly in complex interference scenarios, such as the interference span over the time domain or the number of interference sources is large. To this end, a threshold-free method based on RNN (Recurrent Neural Network) model has been investigated [21], [22]. RNN is a class of neural networks

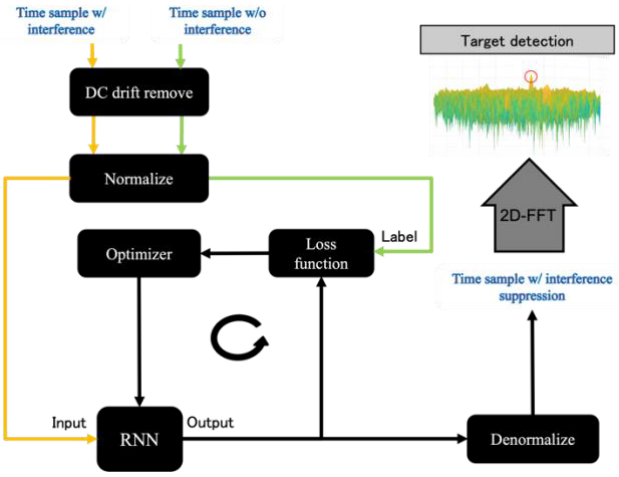

Fig. 4 RNN based wideband interference mitigation method.

where connections between neurons form cycles, which is well-suited for learning from time-series data.

The architecture of the RNN-based interference mitigation method is shown in Fig. 4. During the learning process, the input data and corresponding labels are prepared as pairs. The objective of the learning is to minimize the difference between the label and the output of the model. Specifically, the input $X = [x_1, x_2, \ldots, x_N]$ represents the time sampled beat signal with interference for one chirp, and the label $\hat{Y} = [\widehat{y_1}, \widehat{y_2}, \ldots, \widehat{y_N}]$ represents the beat signal without interference, both under the same target conditions. The loss function L is defined as the Mean Squared Error (MSE) between the output Y and the label $\hat{Y}$ by using the following equation.

$$L = \sum_{1}^{N}(\widehat{y_i} - y_i)^2 \tag{3}$$

The loss is minimized using the Adam optimizer. Finally, as the learning converges, it is expected that the interference can be mitigated in the output samples.

4. Simulation Evaluation

In this section, we address the tradeoff between interference mitigation performance and training time of the RNN model by simulations in a very challenging scenario with up to 7 interfering radars. We consider scenarios with multiple targets and interference resources. Both the transmitting radar and the interfering radar use CS waveforms, but they have different chirp rates. We train and test the RNN model using time samples from various scenarios. In one scenario, the beat signals containing 75 chirps are used for both clean and interfering signals. Each chirp consists of 416 samples. Regarding the simulation environment, a workstation equipped with Intel® Core™ i9-10980XE and NVIDIA RTX A6000 is used. We use MATLAB with Phased Array System Toolbox to generate radar reflected signal, and preprocess the data. Python TensorFlow is used to learn and evaluate the RNN

Table 1 RNN hyperparameter.

Hyperparameter	Value
Learning rate	0.001
Epoch	1000
Hidden state size	100
Number of layers	3
Batch size	128

Table 2 Radar waveform and scenario related parameters.

Parameter	Range
Center frequency	76~78GHz
Distance	1~130m
Velocity	1~50km/h
Chirp period	20~40μs
Sweep bandwidth	100~200MHz
Number of targets	1~2
Number of interferences	1~4

model. The main hyperparameters of the RNN are summarized in Table 1. Specifically, a RNN model with 3 layers with 100 hidden state size in each layer is adopted. Since after the hyper-parameter tuning, we find this setting could achieve the best tradeoff between performance and running time. The radar and scenario-related parameters are summarized in Table 2, which is a standard setting for mmWave radars.

Figure 5 illustrates the time waveform and frequency spectrum in a scenario with 7 interference radars. From the time waveform that shown in Fig. 5(a), we can confirm that the interference covers the entire time domain and the amplitude of it is significantly larger than the signal level of ego radar. By performing FFT, we can obtain the frequency spectrum that shown in Fig. 5(b). It is obvious that the target around 40 m is completely buried by noise. However, by applying the RNN model based interference mitigation, the noise level could be significantly reduced which is even lower than the noise level of the spectrum without interference. However, on the other hand, the downside of the RNN model based method is that the peak level of the target is also reduced to some extent.

Next, we evaluate the achieved SINR of the RNN model based interference mitigation method with up to 7 interfering radars varying with the number of model training scenarios. As shown in Fig. 6. we varied the number of training scenarios as 5, 10, 25, 50, and 100, and use a fixed 20 scenario to evaluate the performance. From the results, it can be observed that the models trained with 25 or more scenarios consistently show an improvement of approximately 15 dB in SINR over the result without interference mitigation. We notice that the gap between with and without interference mitigation becomes larger as the number of interference radars increases.

As a wrap up, we can conclude that the RNN model based method is capable of delivering high performance even in very challenging scenarios with up to 7 interfering radars.

Finally, we evaluate the training time of the model varying with the number of training scenarios and summarize the results in Table 3. It can be observed that although SINR improves significantly when a larger number of training scenarios is used, there is also a substantial increase in the training time of the utilized RNN model. This performance tradeoff becomes significant especially when the RNN model is trained locally in each vehicle.

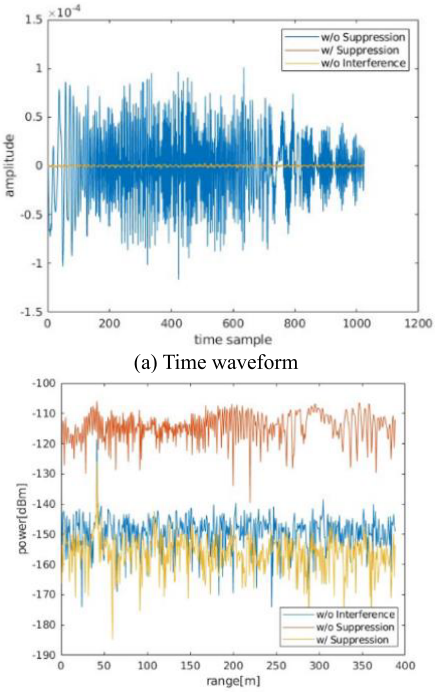

(a) Time waveform

(b) Frequency spectrum

Fig. 5 Interference mitigation performance in a scenario with 7 interfering radars.

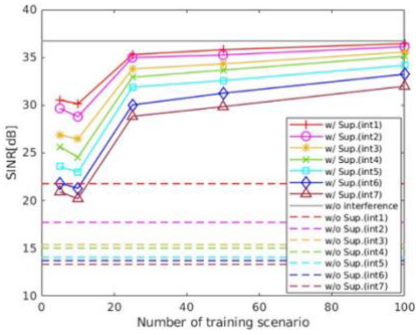

Fig. 6 SINR varying with the number of training scenarios.

Table 3 Training time varying with number of scenarios.

Training scenario	Time
5	1.48h
10	2.95h
25	7.31h
50	14.51h
100	29.01h

5. Experimental Evaluation

5.1 Experimental Scenario and Settings

In order to validate the real-world effectiveness of inter-radar interference mitigation methods, we conducted extensive multi-interference experiments using 77GHz MIMO CS radars. As shown in Fig. 7(a), the inter-radar interference experiments were conducted at the stadium of Nanzan University, Nagoya, Japan. The experimental scenarios are shown in Fig. 7(b). Targets are located at distances ranging from 5 m to 20 m, and 1 to 4 interfering radars are placed at distances from 4 m to 5 m. A trigger pulse generator is used to adjust the timing of the interfering radars to ensure the occurrence of the interference. As shown in Fig. 7(c), 2×4 MIMO CS radars with 2 transmitting antennas and 4 receiving antennas manufactured by Sakura Tech are used. Two series of chirp signals are transmitted in a time-division manner to obtain 8-channel received signals. Each radar is connected to a computer via a PoE interface, and the analysis software shown in Fig. 7(d) is used to observe, record and process the measurement data. Table 4 shows the major radar parameters in the experiment.

(a) Experimental scene

(b) Experiment scenario

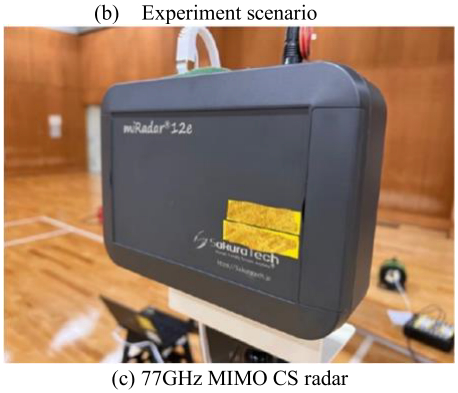

(c) 77GHz MIMO CS radar

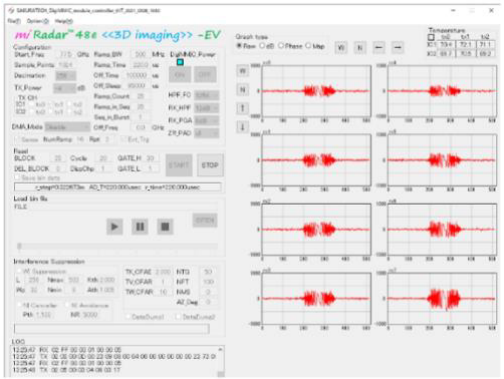

(d) Screenshot of the software

Fig. 7 Inter-radar wideband interference experiment.

We evaluate the performance of the RNN-based interference mitigation method and compare it with existing algorithm-based methods. Regarding the RNN-based method, we prepare 3 different models as follows: a model trained by simulation data with 50 scenarios; a model trained by experimental data with 50 scenarios; and a model pretrained by simulation data with 50 scenarios and then fine-tuned by experimental data with 10 scenarios. For comparison, the envelope detection and sorting based method and the conventional zero suppression method are compared. To perform the evaluations for all the methods, we use 10 experimental data sets that are different from the data used in the training.

5.2 Evaluation Metrics

In this paper, we consider two evaluation metrics which are SINR and MAPE (Mean Absolute Percentage Error). SINR indicates the difference between the power of the peak and noise level, and thus large SINR leads to easy target detection. MAPE indicates the difference of peak positions before and after interference mitigation, and thus small MAPE means less negative affect due to interference mitigation. The calculations of SINR and MAPE are described as follows.

To calculate SINR, first, a reference peak $\hat{p}$ is detected

Table 4 Radar parameters in the experiment.

Parameter	Value
Start frequency	77.5GHz
Chirp period	25,50μs
Sweep bandwidth	1,2GHz
Sampling frequency	26.7,53.3GHz
Number of samples	1024
Number of interferences	1~4
Distance of targets	5~20m
Distance of interferences	4~5m

in the spectrum without interference. Then, in the spectrum with interference under the same target condition, the sample with largest value around reference peak is obtained and set as the peak p. Thereafter, 80 samples around the peak are used as the noise level to calculate the SINR. Finally, the same calculation is performed on all chirps and the finally achieved average SINR can be obtained.

MAPE is calculated using the reference peak $\hat{p}$ in the spectrum that does not include interference and the corresponding peak p in the spectrum that includes interference. Specifically, the MAPE is derived by the following equation.

$$MAPE = \left| \frac{p - \hat{p}}{\hat{p}} \right| \times 100\% \tag{4}$$

The average MAPE over all chirps are evaluated.

5.3 Data Preprocessing

In CS radar, low-frequency amplitude fluctuations, denoted as DC (Direct Current) fluctuations, occur in the beat signal due to phase noise in the PPL circuit that generates the chirp signal. Therefore, instead of directly feeding the measured time samples for learning or evaluation, we remove the DC fluctuations in the waveform first. Specifically, for the beat signal $r(i)(i = 1toN)$ including DC fluctuation, a moving average $D(i)$ for each sample i is obtained using the window width W_l, which is set to 32 in this paper. $D(i)$ is calculated by the following equation.

$$D(i) = \frac{1}{2W_l + 1} \sum_{n=i-W_l}^{i+W_l} r(n) \tag{5}$$

By this method, DC fluctuations are removed by subtracting the moving average $D(i)$ from the beat signal $r(i)$. Figure 8 shows an example of the time waveforms before and after removing DC fluctuations. Finally, the time samples after the DC removal are normalized such that the root sum square of all samples in one chirp is 1.

5.4 Evaluation Results

Figure 9 illustrates the time waveforms of a scenario with one interfering radar, where the target is at 5 m. Specifi-

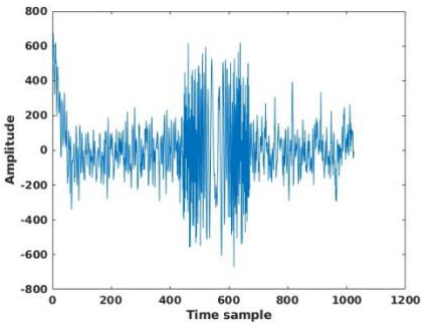

(a) Before DC fluctuation removal

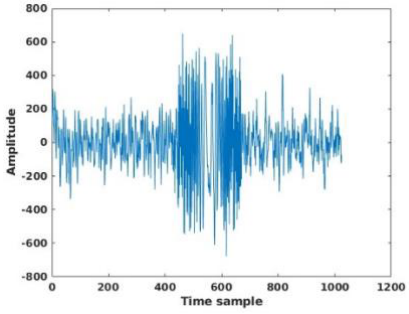

(b) After DC fluctuation removal

Fig. 8 An example of DC fluctuation removal.

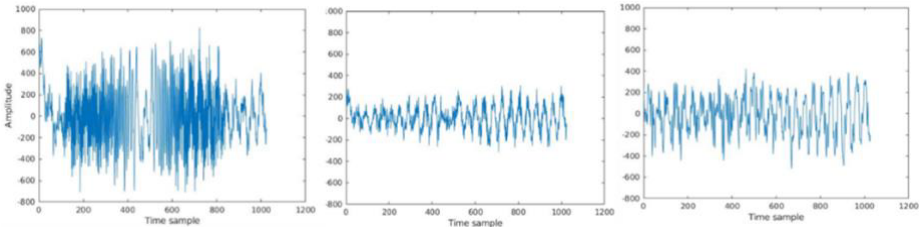

(a)W/o mitigation (b)Simulation model (c)Experimental model

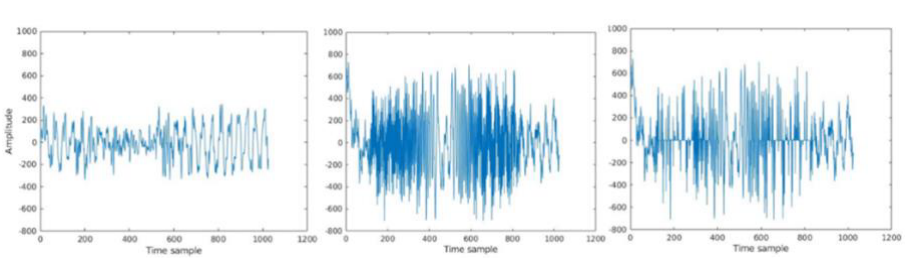

(d)Fine-tuning model (e) Envelope detection and sorting (f) Zero suppression

Fig. 9 Time waveforms for scenario with 1 interfering radar.

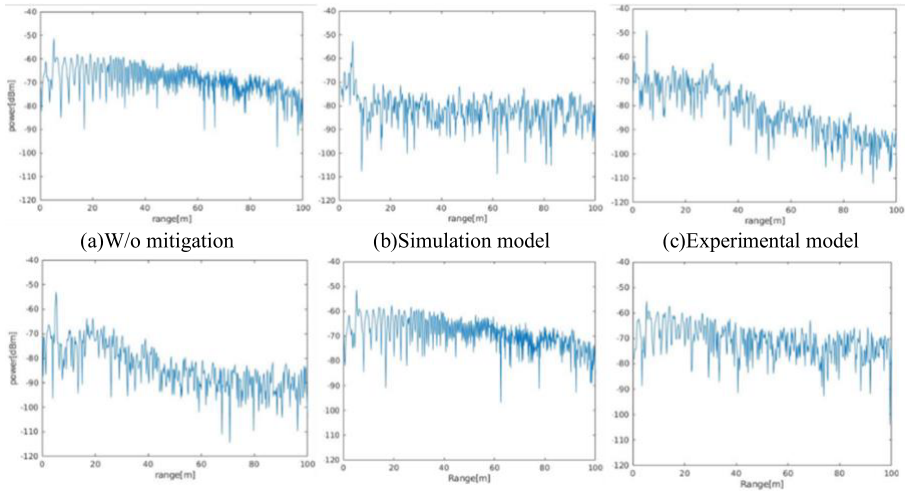

(a)W/o mitigation (b)Simulation model (c)Experimental model

(d)Fine-tuning model (e) Envelope detection and sorting (f) Zero suppression

Fig. 10 Frequency spectrum for scenario with 1 interfering radar.

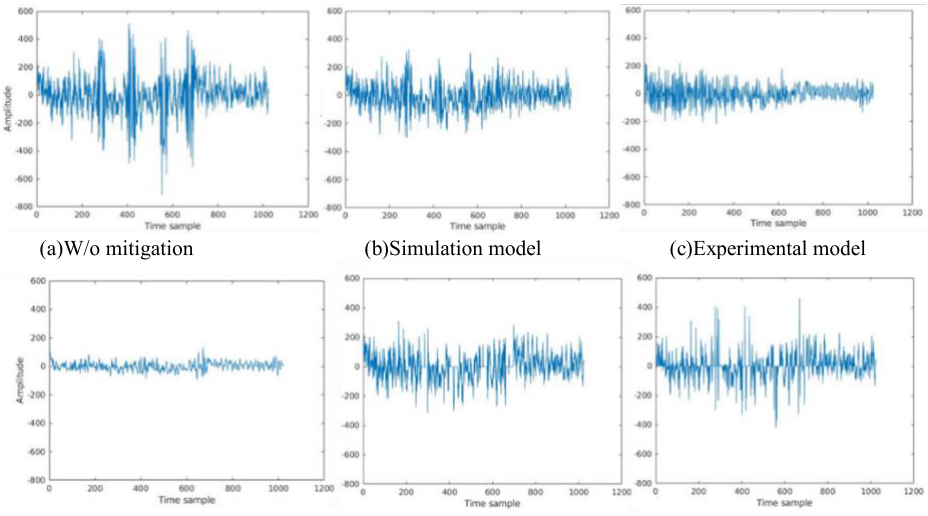

(a)W/o mitigation (b)Simulation model (c)Experimental model

(d)Fine-tuning model (e) Envelope detection and sorting (f) Zero suppression

Fig. 11 Time waveform for scenario with 4 interfering radars.

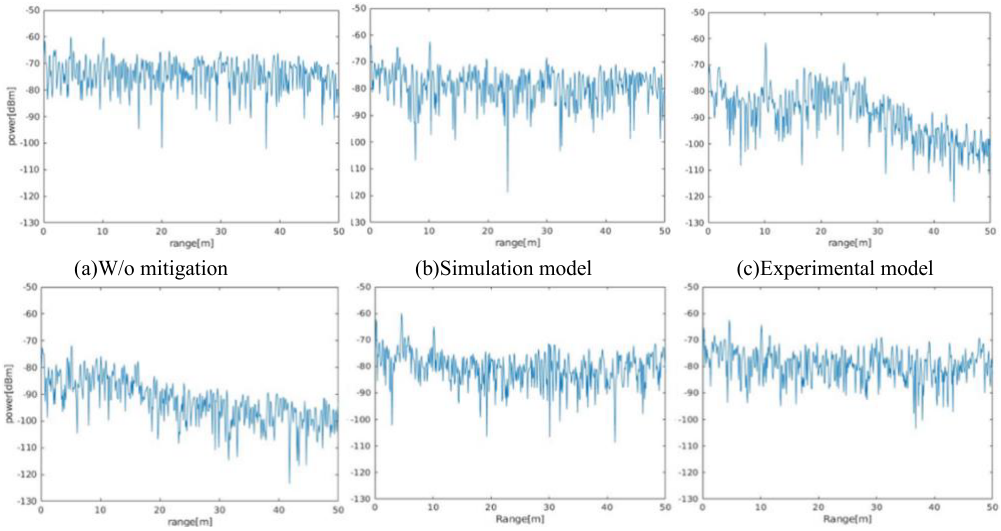

(a)W/o mitigation (b)Simulation model (c)Experimental model

(d)Fine-tuning model (e) Envelope detection and sorting (f) Zero suppression

Fig. 12 Frequency spectrum for scenario with 4 interfering radars.

cally, Figs. 9(a) to (f) show the time waveforms before mitigation, suppressed by a simulation model, suppressed by an experimental model, suppressed by a fine-tuning model, suppressed by the envelope detection and sorting method, and suppressed by conventional zero suppression method, respectively. We can notice that all three RNN-based methods could mitigate the interference signal to some extent, however, two algorithm based methods do not work well. The generated threshold to detect the interference is too large since the interfering signal is too wide.

Figure 10 illustrates the corresponding frequency spectrum. As shown in Figs. 10(a) to (f), it can be confirmed that the interference is well mitigated and the SINR could be improved when the learning models are used. Specifically, when the model is trained by experimental data, the peak power maintains at −50 dBm and the noise level around the peak is reduced to approximately −70 dBm. On the other hand, when the algorithm based methods are used, no significant SINR improvement can be observed.

Figures 11 and 12 show the results for a scenario with 4 interfering radars, where the target is at 10 m. Similar to the results in scenario with one interference, the RNN model trained by experimental data outperforms others. Notice the fine-tuning model works poor in this scenario, the peak at 10 m cannot be detected at all since the signal from ego radar is also mitigated. Improving the performance of fine-tuning model in these kind of challenging scenarios will be our future work.

Next, we evaluate the CDF (Cumulative Distribution Function) of SINR for all methods. Figures 13(a) to (c) show the result for scenarios with target distances at 5, 10, and 15 m, respectively, and Fig. 13(d) displays the average for all scenarios. On average, the RNN based models show high interference mitigation performance, and the model trained by experimental data even outperforms the clean data that does not contain interference. By comparing the results for scenario with different target distances, we notice that the performance improvement by learning based methods over algorithm based methods decrease as the target distance increases. Also, among the three RNN models, the model trained by simulation data had relatively low performance. A possible reason for this is that there was a quite large difference between the parameters settings between experimental and simulation data.

Finally, the MAPE of the peak position before and after interference mitigation is evaluated. Figures 14(a) to (c) display the MAPE of detected peak position for each method in scenarios with targets at 5 m, 10 m, and 15 m. In the target 5 m and 10 m scenarios, the MAPE is lower than 1% for all methods. However, the MAPE increases significantly in the target 15 m scenario. From these results, the learning based methods and algorithm based methods show similar performance in terms of MAPE. In addition, no correlation was found between the SINR performance and MAPE of the peak position.

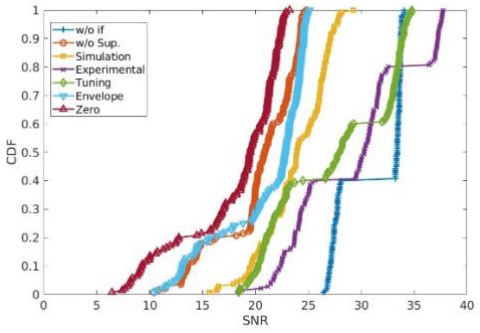

(a) Target 5m

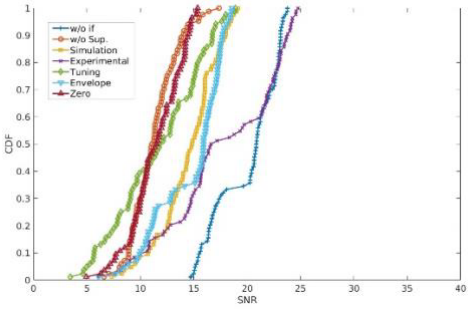

(b) Target 10m

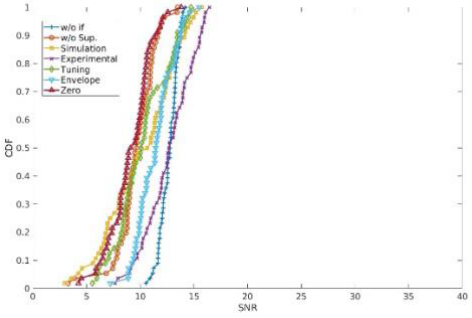

(c) Target 15m

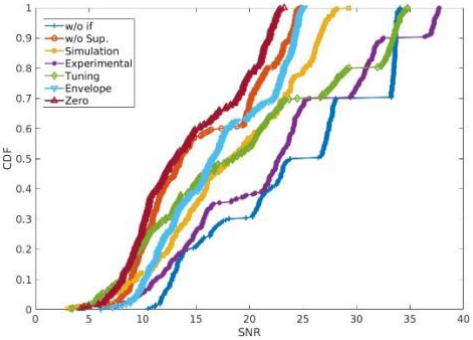

(d) All scenario

Fig. 13 CDF of SINR.

6. Conclusion

In this paper, we evaluate the performance of learning-based inter-radar interference mitigation method in both simulation and experimental environments. By extensive simulation re-

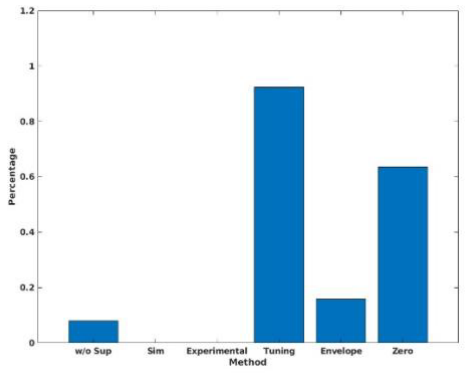

(a) Target 5m

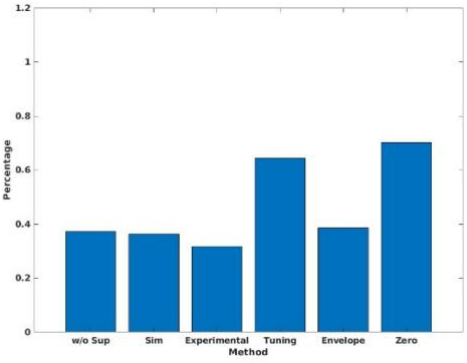

(b) Target 10m

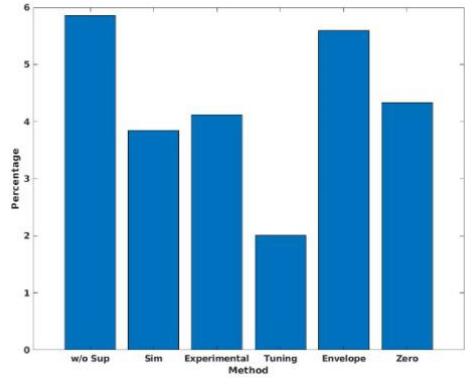

(c) Target 15m

Fig. 14 MAPE of peak position.

sults, we demonstrated that the learning based method can exhibit excellent performance even in very challenging situations where 7 interfering radars are present. Meanwhile, we addressed the tradeoff between SINR improvement and training time, which is extremely important especially in distributed learning environment. Furthermore, we conducted extensive multi-interference experiments by using 77GHz MIMO CS radars to collect real-world data. Performance comparisons in terms of SINR and MAPE were conducted between learning based and algorithm based models by utilizing real-world data. In the future, we will focus on collecting more real data in various environment and improving the accuracy of the model by optimizing the architecture and hyperparameters of the model.

Acknowledgments

This research and development work was supported by the MIC/SCOPE ## JP225003006.

References

[1] M. Nagano, N. Suganuma, K. Yoneda, M. Amro Aldibaja, M. Kishida, and T. Matsumoto, "Object tracking for autonomous vehicles using omni-directional millimeter wave radar system," Transactions of the Society of Automotive Engineers of Japan, vol.48, no.2, pp.411–418, March 2017.

[2] X. Cheng, R. Zhang, and L. Yang, "Wireless toward the era of intelligent vehicles," IEEE Internet Things J., vol.6, no.1, pp.188–202, Feb. 2019

[3] T. Okuda, Y. Makino, M. Umehira, X. Wang, S. Takeda, and H. Kuroda, "Prototype development and experimental performance evaluation of FMCW radar using iterative interference suppression technique," Proc. IET International Conference on Radar Systems (RADAR 2019), Sept. 2019.

[4] C. Waldschmidt, J. Hasch, and W. Menzel, "Automotive Radar — From first efforts to future systems," IEEE J. Microw., vol.1, no.1, pp.135–148, Jan. 2021, doi: 10.1109/JMW.2020.3033616.

[5] R. Sun, J. Sakai, K. Suzuki, J. Zheng, S. Takeda, M. Umehira, X. Wang, and H. Kuroda, "Antenna element space interference cancelling radar for angle estimations of multiple targets," IEEE Access, vol.9, pp.72547–72555, 2021, doi: 10.1109/ACCESS.2021.3078895.

[6] M. Umehira, S. Takeda, X. Wang, and H. Kuroda, "Inter-radar interference mitigation techniques for automotive FMCW radars," IEICE Technical Report, RCS2018-140, Aug. 2018.

[7] S. Rao and A.V. Mani, "Interference characterization in FMCW radars," 2020 IEEE Radar Conference (RadarConf20), Florence, Italy, pp.1–6, 2020, doi: 10.1109/RadarConf2043947.2020.9266283.

[8] D. Ammen, M. Umehira, X. Wang, S. Takeda, and H. Kuroda, "A ghost target suppression technique using interference replica for automotive FMCW radars," 2020 IEEE Radar Conference (RadarConf20), Florence, Italy, pp.1–5, 2020, doi: 10.1109/RadarConf2043947.2020.9266514.

[9] G.M. Brooker, "Mutual interference of millimeter-wave radar systems," IEEE Trans. Electromagn. Compat., vol.49, no.1, pp.170–181, Feb. 2007.

[10] M. Barjenbruch, D. Kellner, K. Dietmayer, J. Klappstein, and J. Dickmann, "A method for interference cancellation in automotive radar," IEEE MTT-S Int. Microw. Symp. Dig., pp.1–4, April 2015.

[11] J. Jung, S. Lim, J. Kim, S.-C. Kim, and S. Lee, "Interference suppression and signal restoration using Kalman filter in automotive radar systems," Proc. IEEE Int. Radar Conf. (RADAR), pp.726–731, April 2020.

[12] T. Shimura, M. Umehira, Y. Watanabe, X. Wang, and S. Takeda, "An advanced wideband interference suppression technique using envelope detection and sorting for automotive FMCW radar," 2022 IEEE Radar Conference (RadarConf22), New York City, NY, USA, pp.1–6, 2022.

[13] Y. Li, C. Wang, F. Li, X. Han, and Y. Song, "An adaptive interference cancellation method for automotive FMCW radar based on waveform optimization," IET International Radar Conference (IET IRC 2020), Online Conference, pp.666–670, 2020, doi: 10.1049/icp.2021.0741.

[14] S. Jin, P. Wang, P. Boufounos, R. Takahashi, and S. Roy, "Spatial-domain object detection under MIMO-FMCW automotive radar interference," ICASSP 2023 - 2023 IEEE International Conference on Acoustics, Speech and Signal Processing (ICASSP), Rhodes Island, Greece, pp.1–5, 2023, doi: 10.1109/ICASSP49357.2023.10095409.

[15] M. Rameez, M. Dahl, and M.I. Pettersson, "Experimental evaluation of adaptive beamforming for automotive radar interference suppression," 2020 IEEE Radio and Wireless Symposium (RWS), San Antonio, TX, USA, pp.183–186, 2020, doi: 10.1109/RWS45077.2020.9049982.
[16] J. Rock, M. Toth, P. Meissner, and F. Pernkopf, "Deep interference mitigation and denoising of real-world FMCW radar signals," Proc. IEEE Int. Radar Conf. (RADAR), pp.624–629, April 2020.
[17] M. Rameez, M. Dahl, and M.I. Petterson, "Autoregressive model-based signal reconstruction for automotive radar interference mitigation," IEEE Sensors J., vol.21, no.5, pp.6575–6586, March 2021.
[18] R. Li, J. Wang, Y. He, Y. Yang, and Y. Lang, "Deep learning for interference mitigation in time-frequency maps of FMCW radars," 2021 CIE International Conference on Radar (Radar), Haikou, Hainan, China, pp.1883–1886, 2021, doi: 10.1109/Radar53847.2021.10028226.
[19] H. Todawat, D. Kakkar, and G. Kaur, "A deep learning based approach on radar interference mitigation for autonomous vehicles," 2022 IEEE 3rd Global Conference for Advancement in Technology (GCAT), Bangalore, India, pp.01–06, 2022, doi: 10.1109/GCAT55367.2022.9972166.
[20] T.-H. Sang, K.-Y. Tseng, F.-T. Chien, C.-C. Chang, Y.-H. Peng, and J.-I. Guo, "Deep-learning-based velocity estimation for FMCW radar with random pulse position modulation," IEEE Sensors Lett., vol.6, no.3, pp.1–4, March 2022, Art no.7000804, doi: 10.1109/LSENS.2022.3156882.
[21] J. Mun, S. Ha, and J. Lee, "Automotive radar signal interference mitigation using RNN with self attention," Proc. IEEE Int. Conf. Acoust., Speech Signal Process. (ICASSP), pp.3802–3806, May 2020.
[22] R. Koizumi, X. Wang, M. Umehira, S. Takeda, and R. Sun, "RNN-based interference suppression method for CS radar: Simulation and experimental evaluations," Proc. International Conference on Artificial Intelligence in Information and Communication (ICAIIC 2023), Feb. 2023.
[23] M. Wagner, F. Sulejmani, A. Melzer, P. Meissner, and M. Huemer, "Threshold-free interference cancellation method for automotive fmcw radar systems," 2018 IEEE International Symposium on Circuits and Systems (ISCAS), IEEE, pp.1–4, 2018.

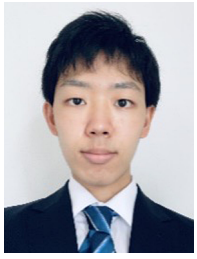

Ryoto Koizumi received the B.E. degree from Ibaraki University in 2022. He is currently a 2nd year master's student in Ibaraki University. His research interest is inter-radar interference suppression technology for in-vehicle radar using machine learning.

Xiaoyan Wang received the B.E. degree from Beihang University, China, and the M.E. and Ph.D. from the University of Tsukuba, Japan. He is currently working as an associate professor with the Graduate School of Science and Engineering at Ibaraki University, Japan. Before that, he worked as an assistant professor at National Institute of Informatics (NII), Japan, from 2013 to 2016. His research interests include networking, wireless communications, cloud computing, big data, security and privacy. He is a member of IEICE and senior member of IEEE.

Masahiro Umehira received the B.E., M.E. and Ph.D. degrees from Kyoto University, Kyoto, Japan in 1978, 1980 and 2000, respectively. Since joining NTT (Nippon Telegraph and Telephone Corporation) in 1980, he has been engaged in the research and development of modem and TDMA equipment for satellite communications, TDMA satellite communication systems, broadband wireless access systems for mobile multimedia services and ubiquitous wireless systems. From 1987 to 1988, he was with the Communications Research Center, Department of Communications, Canada, as a visiting scientist. Since 2006, he has been a professor of Ibaraki University, Ibaraki, Japan. His research interest includes broadband wireless access technologies, wireless networking, cognitive radio, future satellite communication systems and wireless-based ubiquitous systems. He received Young engineer award and Achievement award from IEICE in 1987 and 1999, respectively. He also received Education, Culture, Sports, Science and Technology Minister Award in 2001 and TELECOM System Technology Award from the Telecommunications advancement Foundation in 2003. He is a fellow of IEICE and member of IEEE.

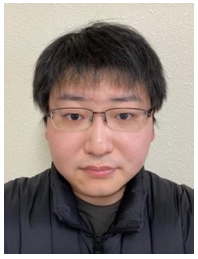

Ran Sun received the B.E., M.E., and Ph.D. degrees in computer and information science from Ibaraki University, in 2016, 2017, and 2020, respectively. Since 2020, he has been an Assistant Professor with Ibaraki University. His research interests include optical wireless communication, error correcting codes, the Internet of Things platform, and vehicle-borne radar. He is a member of IEICE.

Shigeki Takeda received his B.E., M.E. and D.E. degrees in electrical and electronic engineering from Tottori University, Tottori, Japan, in 1996, 1998 and 2000, respectively. Since 2000, he has been with Graduate School of Science and Engineering, Ibaraki University, Ibaraki, Japan, where he is currently a professor. His research interests are in RFID tag, MIMO and adaptive array antenna. He is a member of IEICE.